The clumpiness of molecular clouds:
HCO+ (3–2) survey near Herbig-Haro objects

W. Whyatt[1], J. M. Girart[2], S. Viti[1], R. Estalella[3], and D. A. Williams[1]

[1] Department of Physics & Astronomy, University College London, Gower Street, London WC1E 6BT
e-mail: wwhyatt@star.ucl.ac.uk
[2] Institut de Ciències de l'Espai (CSIC-IEEC), Campus UAB, Facultat de Ciències, Torre C5 - parell 2, 08193 Bellaterra, Catalunya, Spain
[3] Departament d'Astronomia i Meteorologia, Universitat de Barcelona, Martí i Franquès 1, 08028 Barcelona, Catalunya, Spain

ABSTRACT

Context. Some well-studied Herbig Haro objects have associated with them one or more cold, dense, and quiescent clumps of gas. We propose that such clumps near an HH object can be used as a general measure of clumpiness in the molecular cloud that contains that HH object.

Aims. Our aim is to make a survey of clumps around a sample of HH objects, and to use the results to make an estimate of the clumpiness in molecular clouds.

Methods. All known cold, dense, and quiescent clumps near HH objects are anomalously strong HCO+ emitters. Our method is, therefore, to search for strong HCO+ emission as an indicator of a clump near to an HH object. The searches were made using JCMT (for Northern hemisphere objects) and SEST (for Southern hemisphere objects) in the HCO+ (3–2) and also (for SEST observations) $H^{13}CO^+$ (1–0) lines, with some additional searches for methanol and sulphur monoxide lines. The sources selected were a sample of 22 HH objects in which no previous HCO+ emission had been detected.

Results. We find that half of the HH objects have clumps detected in the HCO+ (3–2) line and that all searches in $H^{13}CO^+$ 1-0 lines show evidence of clumpiness. All condensations have narrow linewidths and are evidently unaffected dynamically by the HH jet shock.

Conclusions. We conclude that the molecular clouds in which these HH objects are found must be highly heterogeneous on scales of less than 0.1 pc. An approximate calculation based on these results suggests that the area filling factor of clumps affected by HH objects is on the order of 10%. These clumps have gas number densities of $\gtrsim 3 \times 10^4$ cm^{-2}.

Key words. ISM: abundances — ISM: clouds — ISM: molecules — Radio lines: ISM — Stars: formation

1. Introduction

The clumpy structure of molecular clouds is an important phenomenon that is related both to interstellar dynamics and to the formation of low mass stars occurring within these clouds. However, clumpiness is generally unresolved by single-dish telescopes and can best be detected by interferometric observations such as those of Morata, Girart, & Estalella (2003, 2005) in their studies of a portion of the dark cloud L673 in three molecular lines. Morata et al. showed that there were clear morphological differences for each molecular line observed. In high angular resolution single dish observations of TMC-1 Core D in C_2S lines, Peng et al. (1998) also found that clumps were abundant in the region observed, and were resolved with sizes less than one-tenth of a parsec. Both sets of observations implied that the clumps were transient.

Garrod et al. (2006) adopted the implications of the Morata et al. (2005) observations of clumpiness in a chemical model of a molecular cloud that was regarded as an ensemble of tran-

sient clumps, randomly situated in both space and time. The chemistry was followed in a time-dependent way. These authors showed that this cloud model is able to account in a natural way (based on the time-dependence of the chemistry) for the observed characteristic structures and morphological differences between different species at both low and high angular resolution.

In the present paper, we present an alternative observational approach to the study of clumpiness within molecular clouds. This approach relies on the observational result that some Herbig-Haro objects are found to have associated with them small dense condensations of gas first observed in enhanced emission in lines of HCO+ and NH_3, e.g.: HH 1/2 (Torrelles et al., 1992; Girart et al., 2002, 2005); HH 7-11 (Rudolph & Welch, 1988; Dent et al., 1993); HH 34 (Rudolph & Welch, 1992); NGC 2264G (Girart et al., 2000). In spite of the nearby HH shocks, the regions of enhanced HCO+ emission are found to be quiescent; their temperatures are close to 10 K, and their linewidths are narrow (on the order of 1 km s^{-1}). These regions are much denser than the typical

cloud density, and the observations suggest H_2 number densities on the order of 10^5 cm^{-3}.

The condensations associated with HH objects have also been studied in the case of HH 2 in lines of 12 molecular species (Girart et al., 2002), in addition to HCO$^+$ and NH$_3$. These observations confirm that the condensations are as dense and cold as indicated by the previous HCO$^+$ and NH$_3$ observations. This work also made clear that the chemistry of these condensations is distinct from that of the ambient cloud. Viti, Girart, & Hatchell (2006) showed that this chemical anomaly was shared by at least five other HH objects. While subsequent and more detailed studies of HH 2 (Girart et al., 2005; Lefloch et al., 2005) showed that the region ahead of the shock is more complex than had been previously considered and that some dynamical interaction with the HH shock may be occurring, nevertheless, significant parts of the condensations near HH 2 are confirmed to be quiescent, cold and dense.

Are the condensations associated with HH objects similar to the clumps directly observed by interferometric means in L673? If so, then we may regard HH objects as a probe of clumpiness in molecular clouds, or at least those regions surrounding the HH objects. It is therefore important to determine the extent of clumpiness as revealed by HH objects. Since observations made by many authors over the last three decades all confirm that the condensations associated with HH objects are strong emitters in HCO$^+$, we use strong HCO$^+$ (3–2) emission as a signature of a dense clump in the vicinity of an HH object. We report here the results of an HCO$^+$ (3–2) survey of condensations associated with 22 HH objects. The aim of this work was to determine a measure of the clumpiness in molecular clouds containing HH objects.

In § 2 we describe the HCO$^+$ observations made in the HH objects, and in § 3 we give the results of the data obtained. In § 4 we give a brief discussion of clumpiness deduced from these observations of HCO$^+$ emitting condensations near HH objects, and make some conclusions about the nature of clumpiness in molecular clouds that contain HH objects.

2. Observations

The northern hemisphere observations were carried out with the JCMT telescope on Mauna Kea between December 2002 and August 2003. The JCMT observations were done in typical band 4 weather ($\tau_{230GHz} \sim 0.12$–0.2), with the heterodyne A3 receiver centred at 267.56 GHz for the HCO$^+$ (3–2) line. Additional observations of the CH$_3$OH ($5_n - 4_n$) rotational line were taken in the position of the strongest HCO$^+$ emission for HH 29. The full width at half maximum (FWHM) beam size is $\simeq 20''$ for these two lines. As the cold, quiescent regions produce narrow linewidths ≤ 1 km s^{-1}, the minimum bandwidth of 125 MHz was used to produce a velocity resolution of ~ 0.12 km s^{-1}. This bandwith allows for the detection of the two strongest lines of CH$_3$OH (5_{-1}–4_{-1}, 5_0–4_0). The typical integration time was 4 min per offset for the HCO$^+$ observations and 27 mins per offset for the methanol observations in order to obtain a baseline rms of 0.15 K and 0.05 K respectively. Main beam efficiency for the HCO$^+$ (3–2) line was 0.69.

The southern hemisphere observations were carried out with the SEST on La Silla in January 2003. In the SEST observations we used dual receiver capability to observe simultaneously the HCO$^+$ (3–2) and the H^{13}CO$^+$ (1–0) lines. We used an integration time of 6 min per offset, which yielded an average baseline RMS noise of 0.2 and 0.05 K, at a velocity resolution of 0.2 kms^{-1}, for the HCO$^+$ (3–2) and H^{13}CO$^+$ (1–0) lines, respectively. The FWHM beam size is $\simeq 20''$ and $54''$ for these two lines, respectively. In certain cases, but only if observations of HCO$^+$ (3–2) were successful, additional simultaneous observations of CH$_3$OH (2_n–1_n) and SO (6_5–5_4) were undertaken. To reach an average baseline RMS noise of 0.03 K, at a velocity resolution of 0.1 km s^{-1}, required a typical integration times of 18 mins per offset. Main beam efficiency for the HCO$^+$ (3–2), H^{13}CO$^+$ (1–0), CH$_3$OH (2_n–1_n) and SO (6_5–5_4) lines were 0.42, 0.75, 0.72 and 0.52, respectively.

A successful detection has been defined as a 3σ detection at a velocity resolution of 0.2 km/s, a tentative detection as a signal that is above 2σ. The data were processed using 'CLASS' from the 'GILDAS' software package. Gaussian fits were attempted within an appropriate velocity window close to the V_{LSR} of the region. These velocities are typically within 1 km/s of the known V_{LSR} for the surrounding cloud from the literature.

The sample was selected according to the following criteria: (i) in order to avoid emission from dynamically affected material, we selected HH objects located at the end of the jet, (ii) usually several HH objects are found in the same region (e.g. there are 36 known HH objects in NGC 1333); we selected one HH object per outflow (except for HH 38 and HH 43), to avoid the bias of one region being particularly clumpy with respect to the norm, (iii) we limited our sample to HH objects that are clearly embedded in a dark molecular cloud and, to our knowledge, outside obvious star forming regions, (iv) where possible, we chose HH objects for which CCD images were available from the literature, in order to aid the interpretation of the spatial distribution of the emission. The offset positions from the HH objects were chosen on the basis of known HCO$^+$ clumps ahead of well studied HH objects such as HH 2, which are usually found at a distances of $\lesssim 0.1$ pc downstream of the HH object. However it is important to note that clump does not have to be directly ahead of the HH object. In any case the direction and orientation of the jet is often not known with great certainty, nevertheless the clump is ahead of the HH object in the sense that it has yet to be reached by the jet, and thus has not been dynamically effected by the HH object.

The sources were observed in the HCO$^+$ (3–2) line for numerous offsets around a sample of HH objects. The specific offset positions were kept flexible during our observations so if emission was seen we would be able to adapt the observing procedure to allow us explore this extent of this emission, within the constraints of our available time for each source.

Table 1 shows the list of the HH objects, their position, the v_{LSR} of the molecular cloud, the name of the region and its distance, the distance between proposed exciting source and the HH object, the distance between the HH object and the peak emission seen in HCO$^+$ (3–2) and finally the suspected exciting source of the HH object.

Table 1. Source List. JCMT and SEST. General Information. Column (7) lists the distance between the exciting source and the HH Object. Column (8) lists the distance between the proposed HH Object and the peak emission of HCO⁺ (3–2) seen. 'N/A' indicates that the exciting source is not known and no values can be deduced, whereas a '–' indicates that no HCO⁺ emission was seen.

Object	RA (J2000) (h m s)	Dec (J2000) (° ′ ″)	V_{LSR} (km s^{-1})	Location	Distance (pc)	Dist. source to HH (pc)	Dist. HH to HCO⁺ (pc)	Proposed Exciting Source[a]
HH 267	03 24 03.0	+31 00 29	4.5	L1448	300	2.53	–	L1448C
HH 268	03 24 22.1	+30 48 11	4.5	L1448	300	1.35	–	L1448 IRS1
HH 337A	03 28 26.3	+31 25 53	4.0	NGC 1333	300	0.99	0.03	333 star
HH 278	03 26 59.4	+30 25 58	7.0	L1455/L1448	300	2.47	–	L1448NB
HH 366	03 48 29.8	+32 55 36	5.0	Barnard 5	300	1.28	0.01	B5 IRS 1
HH 427	03 30 37.7	+30 21 56	6.0	Barnard 1	300	N/A	N/A	Not known
HH 211	03 43 56.8	+32 00 50	9.2	IC 348	300	0.08	0.01	HH 211-mm
HH 462	03 54 05.0	+38 10 35	−3.5	Perseus	300	0.01	0.04	IRAS 03507+3801
HH 362A	04 04 24.1	+20 20 41	7.2	L1489	140	0.20	–	IRAS 04106+2610
HH 464	04 10 42.4	+38 07 39	−3.5	L1473	350	0.07	0.05	PP 13N
HH 276	04 22 07.3	+26 57 26	6.5	Taurus-Auriga	140	1.80	–	IRAS 04189+2650
HH 29	04 31 27.6	+18 06 24	6.6	L1551	140	0.11	0.01	L1551 IRS 5
HH 240	05 19 40.7	−05 51 44	8.5	L1634	460	0.28	0.11	IRAS 05173−0555
HH 43	05 38 10.4	−07 09 25	8.5	L1641	460	0.57	0.17	IRAS 05355−0709C
HH 38	05 38 21.8	−07 11 38	8.5	L1641	460	1.06	0.07	IRAS 05355−0709C
HH 272	06 12 48.4	−06 11 21	11.0	L1646	830	0.46	0.08	IRAS 06103−0612
HH 47C	08 25 33.0	−51 01 37	6.0	Gum Nebula	450	0.26	–	HH 46/47 IRS
HH 75	09 11 38.5	−45 42 28	−0.9	Gum Nebula	450	–	–	IRAS 09094−4522
HH 49	11 06 00.1	−77 33 36	5.3	Cha I	160	2.69	–	Cha-MMS1
HH 52-53	12 55 06.4	−76 57 46	4.0	Cha II	165	1.39	–	IRAS 12496−7650
HH 54	12 55 49.5	−76 56 08	4.0	Cha II	165	1.90	–	IRAS 12496−7650
HH 77	15 00 49.0	−63 07 46	−5.0	Circinus	700	0.63	0.06	IRAS 14564−6254

[a] References: HH29: Moriarty-Schieven et al. (2006); HH38–43: Stanke et al. (2000); HH49: Reipurth, Nyman, & Chini (1996); HH52–53 & HH54: Knee (1992); HH47: Sahu, Sahu & Pottasch (1989); HH75 & HH77: Cohen (1990); HH211: McCaughrean, Rayner, & Zinnecker (1994); HH240: Davis et al. (1997); HH267: Bally et al. (1997); HH268: Eislöffel (2000); HH272: Carballo & Eiroa (1992); HH276: Wu et al. (2002); HH278: Eislöffel (2000); HH337A: Bally, Devine, & Reipurth (1996); HH362: Alten et al. (1997); HH366: Bally, Devine, & Alten (1996); HH427: Yan et al. (1998); HH462 & HH464: Aspin & Reipurth (2000)

3. Results

In total, we observed 12 northern hemisphere objects with the JCMT and a further 10 southern hemisphere sources with the SEST (see Table 1 for details). In this section we will briefly describe our source sample and report our detections, if any, for each source, before analysing the emission seen. Figures 1 to 12 show the HCO⁺ (3–2) spectra (and H^{13}CO⁺ for the SEST sample) of the sources with detected emission. Figure 13 shows detections of the CH$_3$OH (2_n–1_n) line. No detections were made in the SO line.

3.1. Details of sources

HH 29: A bright bow shock situated in the large outflow 0.11 pc from the binary, L1551 IRS 5 first seen by Herbig (1974). More recent observations have identified a second outflow from neighbouring L1551 NE with the same orientation as the IRS 5 flow and which is easily confused with the original flow. Because of this, it is unknown which source is powering HH 29, although it is now more commonly thought to be L1551 NE due to deep narrow band images and proper motion measurements of HH 29 (Moriarty-Schieven et al., 2006). The HCO⁺ (3–2) line is detected in all the three offsets (Figure 1).
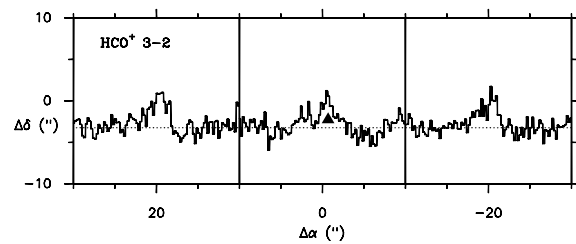

Fig. 1. Spectra of the HCO⁺ (3–2) emission HH 29, observed with JCMT. The horizontal and vertical axes shows the offset position (with respect to the HH object) of the observed spectra. The temperature scale for the spectra is the same for all the figures showing the HCO⁺ (3–2), ranging from T_{mb} = −1.0 to 2.0 K. The HCO⁺ spectra have a velocity resolution of 0.18 km s^{-1}. These spectra have the same velocity range, with a width of 16 k ms^{-1} centered at the systemic velocity of the molecular cloud (this also applies for the H^{13}CO⁺ spectra shown in other figures). The triangle marks the position of the HH object.

This yields to a lower limits for the emission scale of about 0.04 pc.
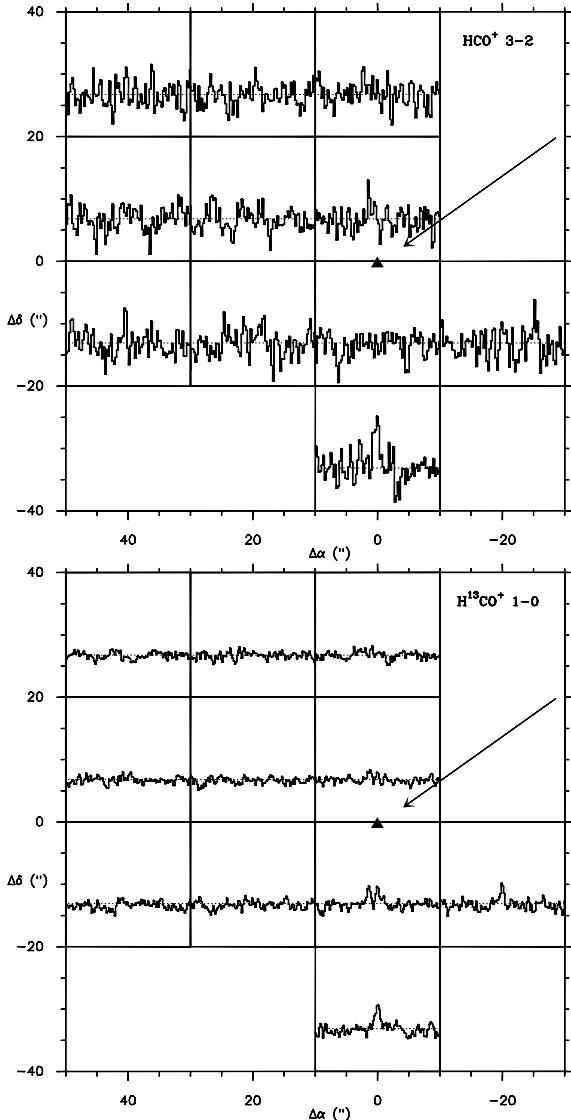
Fig. 2. Spectra of the HCO$^+$ (3–2) (top) and H^{13}CO$^+$ (1–0) emission (bottom) ahead of HH 38, observed with SEST. The temperature scale is the same for all the figures showing the H^{13}CO$^+$ spectra, ranging from T_{mb} = −0.5 to 1.0 K. The H^{13}CO$^+$ spectra have a velocity resolution of 0.15 km s^{-1}. The arrow shows the direction of the outflow and the triangle marks the position of the HH object.

HH 38 & HH 43: Discovered by Haro (1953), both are part of the same HH flow driven by IRAS 05355−0709C, also known as HH 43 MMS1, which also powers HH 64 (Stanke et al., 2000). HH 43 is closer to the source with a projected distance of 0.57 pc, whilst the terminating object, HH 38, is a further 0.5 pc downstream. We detect HCO$^+$ (3-2) in both HH 38 and HH 43, in a single position, suggesting a compact emitting region. However, the detection towards HH 43 is 47″ south (0.1 pc) of knots E and F.

HH 47C: Along with HH 46, HH 47 is a large, well collimated bipolar outflow embedded in the Bok globule ESO 210-6A. Unlike the brighter HH 47A and the older and larger HH 47D, HH 47C is powered by a faint counter-jet and is lo-

cated approximately 0.26 pc from the central source. It was first discovered by Schwartz (1977). We report no detections in the eleven positions observed.

HH 49: Discovered by Schwartz (1977) and along with its close companion HH 50, they are the brightest shocks in the Cha I cloud. Located south of the reflection nebula Ced 110, they trace a large bow flowing out from that region. The observations of Reipurth, Nyman, & Chini (1996) and Bally et al. (2006) indicate that Cha-MMS1 is the driving source - located 0.47 pc upstream from HH 49. We report no detection in any of the 22 observed positions.

HH 52–53 & HH 54: Again first identified by Schwartz (1977), these sources seem to form a chain heading in a north east direction as part of a bow shock driven by IRAS 12496−7650 (0.67 pc southwest). However, Knee (1992) proposed that HH 52–53 and HH 54 are independent HH objects and that they are powered by closer exciting source. HH 54 is spatially coincident with a weak IR source, IRAS 12522−7640, which has also associated a monopolar, blueshifted outflow. HH 52–53 is possibly powered by another weak IR source, IRAS 12522−7641. We found no HCO$^+$ around these HH objects.

HH 75: This is a complex chain of knots located at the southern edge of the irregular cloud S114. Observations of associated nebulous stars by Herbst (1975) indicate the closer Gum Nebula is the host to the objects - as such Cohen (1990), put forward IRAS 09094−4522 as the source located 1.1 pc away. No emission was detected.

HH 77: First identified by Reipurth & Graham (1988), this is a small curved object near several possible powering IRAS sources. Cohen (1990) put forward IRAS 14564−6254 (located 0.4 pc to the WNW) as the powering source due a streamer connecting the two objects. Interestingly the orientation of the bow-shock puts the source in the opposite direction to the IRAS source. This implies that the flow may be colliding with dense clumps and is in the process of flowing around it (Schwartz, 1978). There are 4 detections (≥ 3 σ) in the HCO$^+$ 3–2 line that are clearly detected in the H^{13}CO$^+$ 1–0

HH 211: Discovered by McCaughrean, Rayner, & Zinnecker (1994), HH 211 features a relatively small but highly collimated, bipolar jet (0.16 pc long), seen in molecular hydrogen (IR), and a molecular outflow, both powered by a cold sub-mm source. For HH 211, HCO$^+$ (3–2) emission was seen in each position observed (although falling in intensity with distance from the bow shock) - as such, emission will extend outside the region observed, so we calculate a minimum size of 0.1 pc.

HH 240: First seen by Cohen (1980) under the name RNO 40, it is a chain of HH knots with a bright central core. Hodapp & Ladd (1995) and Davis et al. (1997) infrared H$_2$ observations indicate that HH 240 forms a highly symmetric bipolar outflow with the much fainter HH 241, placing IRAS 05173−0555 as the source 0.28 pc away. HH 240 appears to have a relatively small clump in HCO$^+$ (3–2) of approximately 0.07 pc in length.

HH 267: First discovered by Bally et al. (1997), HH 267 is an extended cluster of knots. L1448C is the likely source of HH 267, as it lies on the axis of its outflow and because the
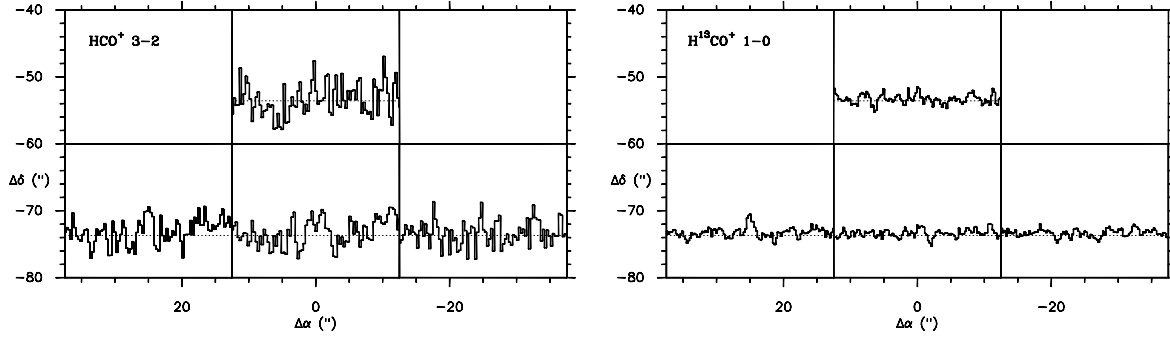
Fig. 3. SEST spectra of the HCO⁺ (3–2) and H¹³CO⁺ (1–0) ahead of HH43. The position offsets are with respect to the brightest knot in HH 43.
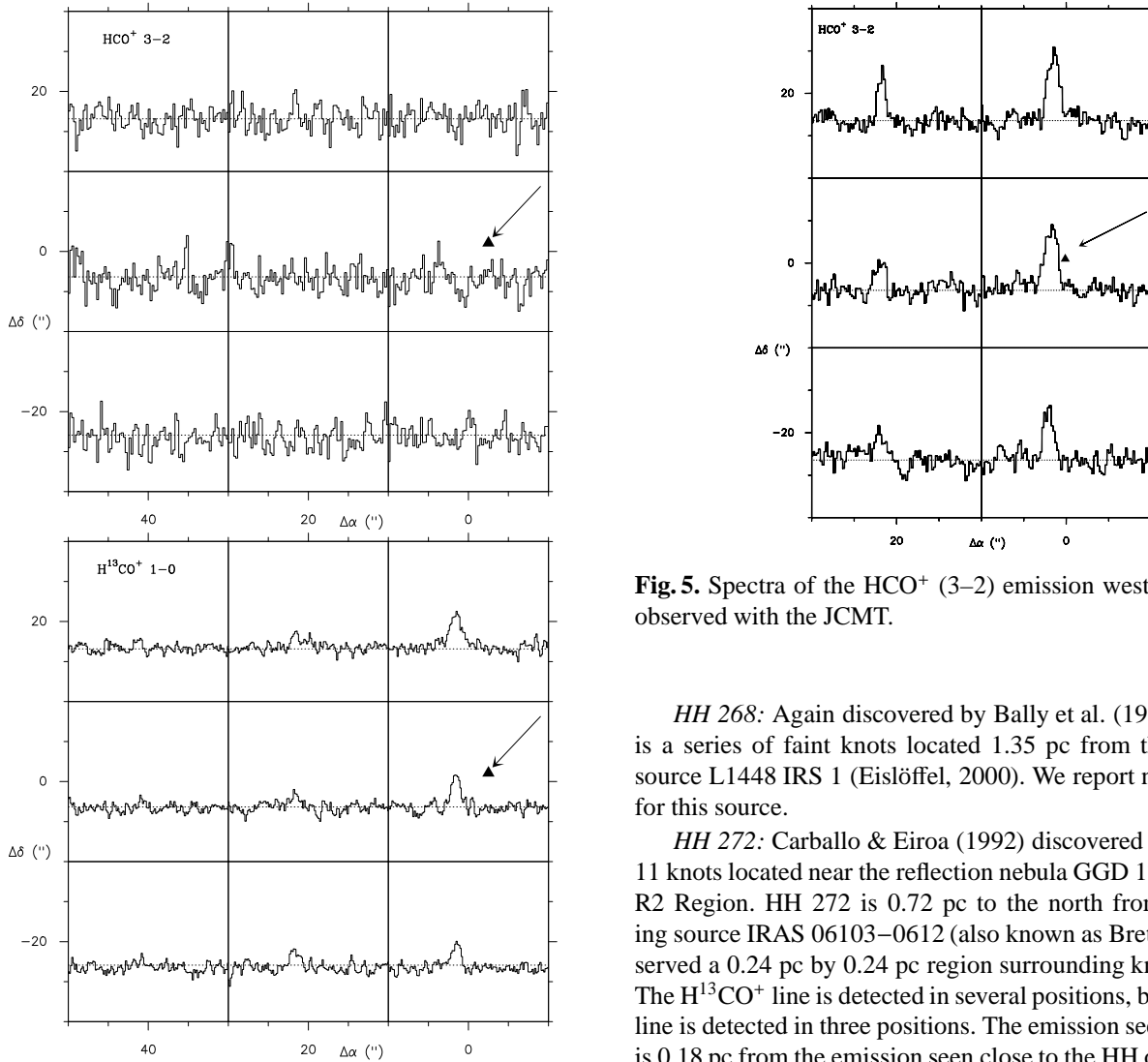

Fig. 4. Spectra of the HCO⁺ (3–2) (top) and H¹³CO⁺ (1–0) (bottom) emission east of HH 77, observed with SEST.
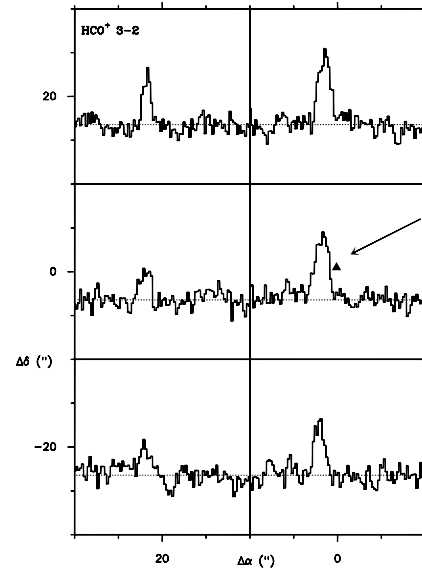

Fig. 5. Spectra of the HCO⁺ (3–2) emission west of HH 211, observed with the JCMT.

HH 268: Again discovered by Bally et al. (1997), HH 268 is a series of faint knots located 1.35 pc from the powering source L1448 IRS 1 (Eislöffel, 2000). We report no detections for this source.

HH 272: Carballo & Eiroa (1992) discovered this chain of 11 knots located near the reflection nebula GGD 17 in the Mon R2 Region. HH 272 is 0.72 pc to the north from its powering source IRAS 06103−0612 (also known as Bretz 4). We observed a 0.24 pc by 0.24 pc region surrounding knots I and H. The H¹³CO⁺ line is detected in several positions, but the HCO⁺ line is detected in three positions. The emission seen to the SW is 0.18 pc from the emission seen close to the HH object and so may be tracing another unrelated clump or extended emission.

HH 276: Originally discovered by Eislöffel & Mundt (1998), it is a series of 4 knots (A to D) that are perpendicular to the far larger Tau B outflow. It is centered roughly 60" (0.04 pc) northeast of FS Tau B, with no known exciting source. The knots broaden to the SE implying the source is NW of HH 276. Wu et al. (2002) put forward IRAS 04189+2650 as the powering source, 1.8 pc away. We obtained no detections for this source.
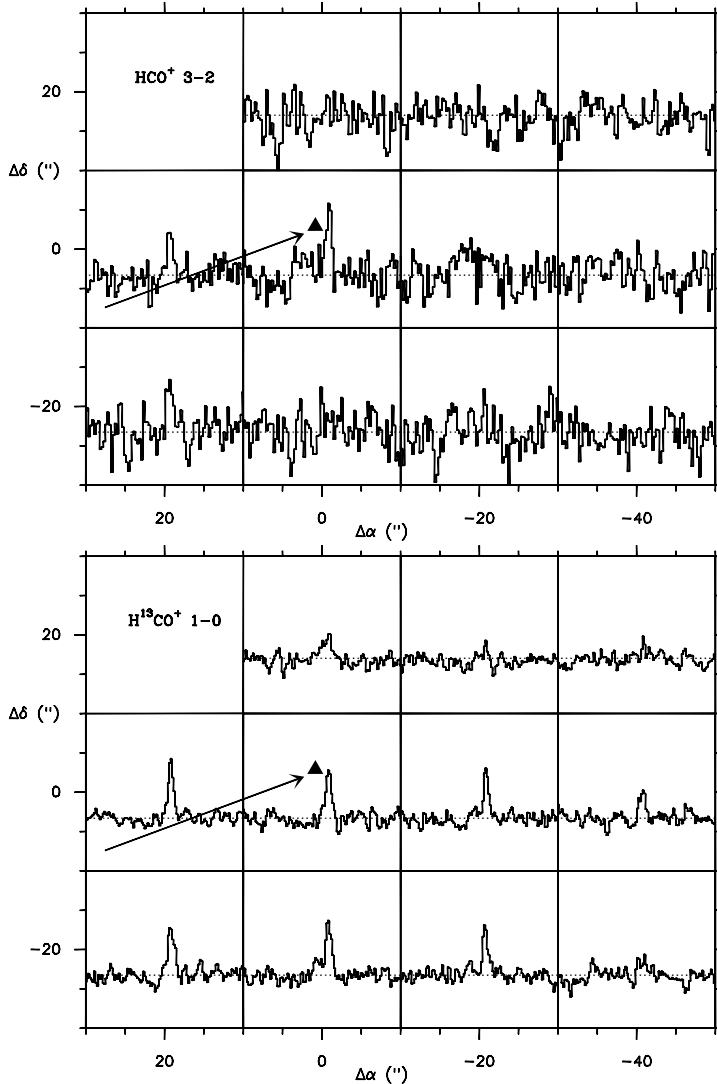
terminal velocity of this outflow is consistent with the velocity of HH 267. The outflow from L1448C is believed to be 0.71 pc long, whilst if it powers HH 267 this extends the flow to a total length of 2.5 pc. We report no detections for this source.

Fig. 6. Spectra of the HCO$^+$ (3–2) (top) and H^{13}CO$^+$ (1–0) emission (bottom) ahead of HH 240, observed with SEST.

Fig. 7. Spectra of the HCO$^+$ (3–2) (top) and H^{13}CO$^+$ (1–0) emission (bottom) ahead of HH 272, observed with SEST.

HH 278: this is a large diffuse object, consisting of at least 3 knots. First seen by Bally et al. (1997), it is located roughly equidistant from L1448 and L1455. The exciting source has not been confirmed - although the outflow from L1448-N(B) (Eislöffel, 2000) is the most likely source as the HH 278 and the outflow are aligned - despite the large 2.47 pc distance between them. No detections were made.

HH 337A: This is an HH extended in the north-south about 6′ west of the HH 333 jet in NGC 1333 (Bally, Devine, & Reipurth, 1996). HH 337A may be part of this HH system, in which case the exciting source would be the 333 star, but this remains to be confirmed. Of the six positions observed, only one shows emission, which appears to be located ahead of the HH 337, if this object belongs to the HH 333 jet (Fig. 8). Thus, HH 337 is a good candidate for compact emission.

HH 362A: First presented in Alten et al. (1997). One of a pair of faint diffuse HH objects in the L1489 cloud, located 0.2 pc from IRAS 04106+2610. No detections were made.
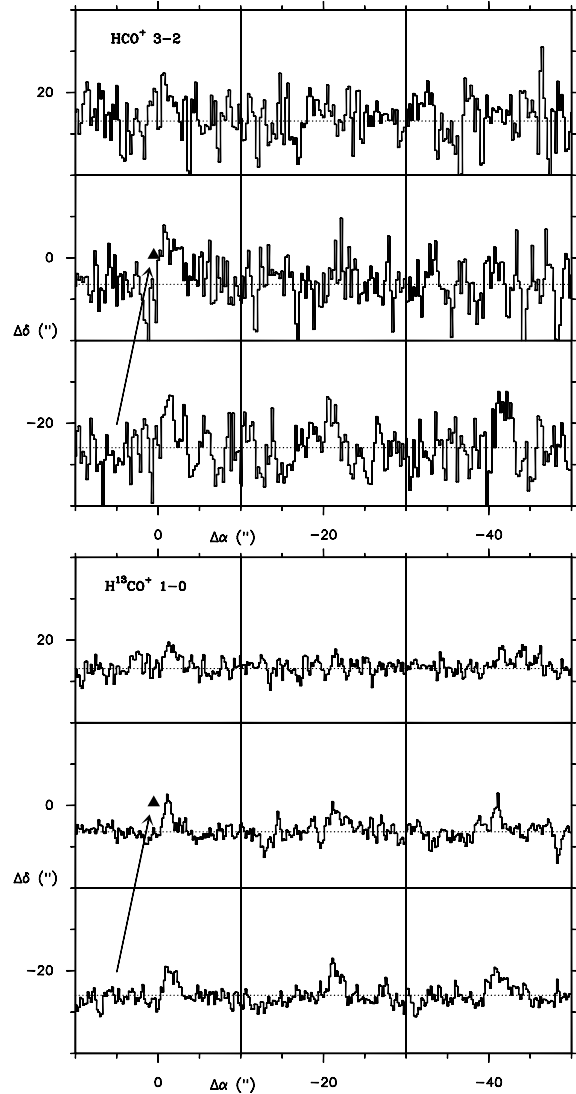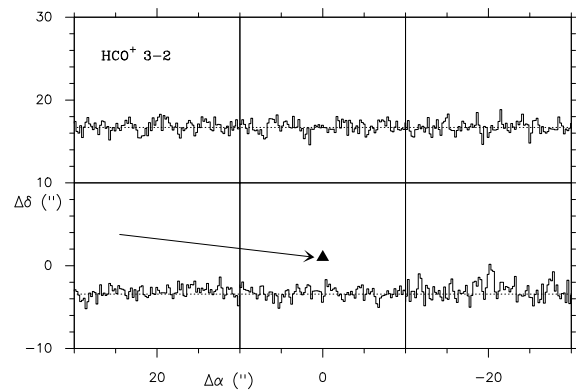

Fig. 8. JCMT Spectra of the HCO$^+$ (3–2) emission surrounding HH 337A. The arrow line shows the tentative exciting source suggested by Bally, Devine, & Reipurth (1996). (Note: HH 337A should not be confused with HH 337 discovered by Noriega-Crespo (2002), which is associated with the Cep E molecular).
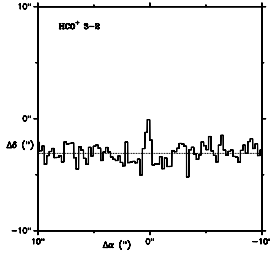
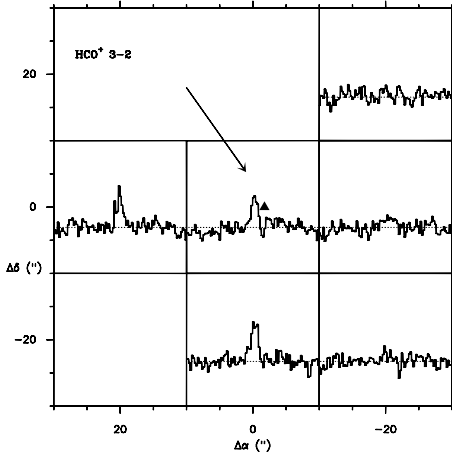**Fig. 9.** JCMT Spectra of the HCO⁺ (3–2) emission toward HH 366.

Fig. 10. JCMT Spectra of the HCO⁺ (3–2) emission surrounding HH 427. The arrow marks the location of the nearest possible source, IRAS 03271+3013, though it unlikely to be responsible (Yan et al., 1998).

Fig. 11. JCMT Spectra of the HCO⁺ (3–2) emission surrounding HH 462.
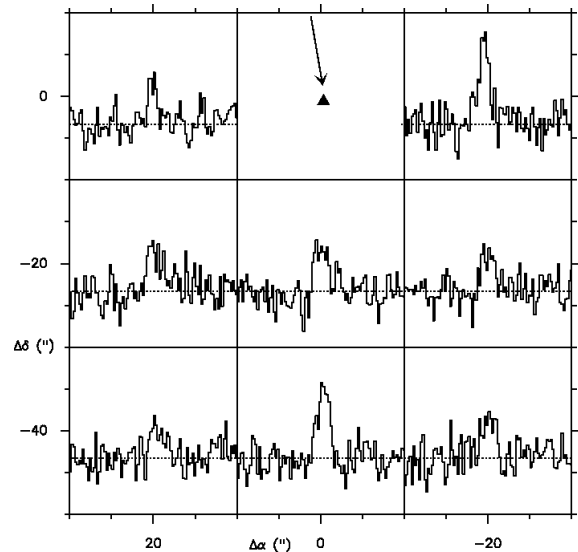
Fig. 12. JCMT Spectra of the HCO⁺ 3–2 emission surrounding HH 464.

HH 366: Driven by the protostar B5-IRS 1 in the parent dark cloud Barnard 5, HH 366 is a parsec scale bipolar outflow discovered by Bally, Devine, & Alten (1996). It is 2.2 pc in length at a distance of 350 pc. HH 366 shows emission in HCO⁺ 3–2 in the only position observed. We observed ahead of knot E2

HH 427: this object was first presented by Yan et al. (1998) and it is located in the Barnard 1 Dark Cloud. The closest source is IRAS 03271+3013, however its bipolar outflow extends from the NE to SW whilst HH 427 is located 0.08 pc SE of the YSO. As such, and with no other likely sources, the exciting source remains unknown. The HCO⁺ is detected in three positions around HH 427 (Fig. 10), with the three positions west to HH 427 showing no emission. The lower limit for the size of the HCO⁺ emission is about 0.05 pc. Assuming that the HCO⁺ is ahead of HH 427, then Figure 10 suggests that the exciting source should be located roughly north or west of HH 427.

HH 462: Discovered by Aspin & Reipurth (2000), it is a small outflow along the symmetry axis of cometary nebulae PP 11 and illuminated by the embedded IRAS 03507+3801 source just 0.01 pc distant. HH 462 shows emission in HCO⁺ (3–2) extending north and east of the HH object, spatially coincident with the center of the optical nebulosity where the YSO is embedded. All emission seen has a double peaked structure.
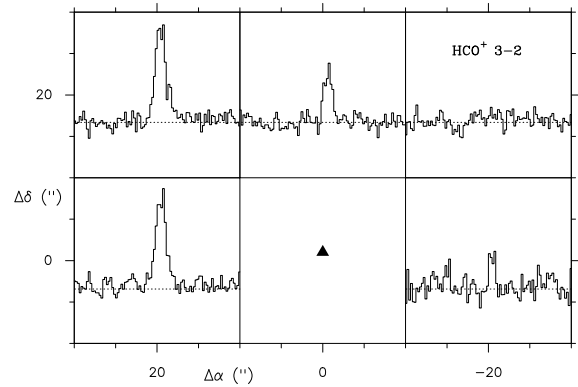
All these indicate that the emission may be tracing the dense circumstellar envelope around the known embedded Class I source (Aspin & Reipurth, 2000). As such it has been excluded from the results presented.

HH 464: Discovered by Aspin & Reipurth (2000), HH 464 is made up of a curved chain of 5 HH knots It appears to be powered by the T Tauri star PP 13N, as the chain is roughly perpendicular to the expected outflow from PP 13S, which is responsible for the nearby HH 463. We observed downstream of knot E, which is 0.07 pc (40″) south from PP 13N. We find emission extending over a region of 0.1 by 0.1 pc, strong HCO⁺ (3–2) lines are seen in every offset, this only defines the minimum size of the region to be 0.14 pc. Interestingly, the two strongest lines are separated by 0.07 pc, with weaker emission seen in the other offsets.

3.2. Survey results

Table 2 details the HCO⁺ (3–2) results for all sources. Column 2 lists for each source, the total number of offsets in which emission was observed in the region surrounding the HH ob-
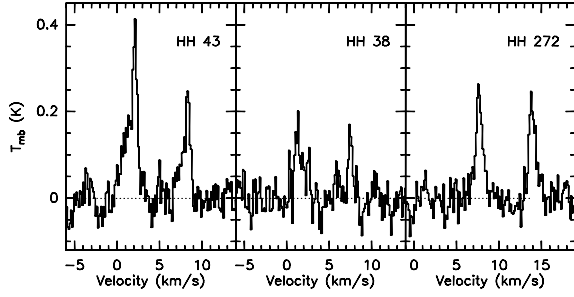
Fig. 13. Spectra of the CH_3OH (2_n-1_n) ahead of HH 43, HH 38 and HH 272, observed with SEST. The offset positions for these spectra are $(0'', -50'')$, $(0'', 10'')$ and $(0'', 0'')$, respectively.

Table 2. HCO^+ (3–2) survey results from both the JCMT and SEST

Object	Positions[a]		Area[b]	T_{mb}	ΔV
	Obs	Det	(pc^2)	(K)	(km s^{-1})
HH 29	3	3	4.3×10^{-4}	0.6±0.1	1.8±0.2
HH 38	11	1	1.7×10^{-2}	1.2±0.3	0.9±0.2
HH 43	4	1	6.3×10^{-3}	0.6±0.2	0.7±0.2
HH 47C	11	0	1.7×10^{-2}	< 1.4	$\cdots$
HH 49	22	0	4.2×10^{-3}	< 0.6	$\cdots$
HH 52-53	9	0	1.8×10^{-3}	< 2.4	$\cdots$
HH 54	12	0	2.4×10^{-3}	< 0.7	$\cdots$
HH 75	9	0	1.4×10^{-2}	< 0.8	$\cdots$
HH 77	9	4	3.3×10^{-2}	1.1±0.3	1.6±0.2
HH 211	6	6	4.0×10^{-3}	1.2±0.1	1.4±0.1
HH 240	11	3	1.7×10^{-2}	1.4±0.3	0.6±0.1
HH 267	6	0	4.0×10^{-3}	< 0.38	$\cdots$
HH 268	3	0	2.0×10^{-3}	< 0.56	$\cdots$
HH 272	9	3	4.6×10^{-2}	1.1±0.4	0.8±0.3
HH 276	6	0	8.7×10^{-4}	< 0.53	$\cdots$
HH 278	6	0	4.0×10^{-3}	< 0.43	$\cdots$
HH 337A	6	1	4.0×10^{-3}	0.5±0.2	0.5±0.1
HH 362A	6	0	8.7×10^{-4}	< 0.46	$\cdots$
HH 366	1	1	6.7×10^{-4}	0.5±0.1	0.3±0.1
HH 427	6	3	4.0×10^{-3}	0.9±0.1	0.9±0.1
HH 462	5	4	3.3×10^{-3}	2.0±0.2	1.0±0.1
HH 464	8	8	7.2×10^{-3}	1.1±0.1	1.2±0.1

[a] Obs: n^o of positions observed, Det: n^o of positions with $\geq 3\sigma$ detections.

[b] The area covered by the observations around the HH object

ject. Column 3 lists the number of offsets in which emission was seen. Column 4 indicates the total area we mapped for emission. A full mapping of the suspected region for each source was not possible due to time constraints and the differing area on the sky covered by the $20''$ beam for sources at different distances. In addition as the orientation of the exciting source and the direction of both the outflow and the UV illumination are not known with certainty, and as such the region being observed is not always located exactly ahead of the HH object. The remaining columns list the peak main beam temperature (5) and the half-power line width (6). The SEST observation of $H^{13}CO^+$ (1–0) is similarly detailed in Table 3. For non-detections, upper limits on the line intensities are given by

Table 3. $H^{13}CO^+$ (1–0) survey results from SEST.

Object	Positions[a]		T_{mb}	ΔV
	Obs	Det	(K)	(km s^{-1})
HH 38	11	3	0.28±0.05	0.9±0.1
HH 43	4	1	0.21±0.04	0.6±0.1
HH 47C	11	0	< 0.23	$\cdots$
HH 49	22	0	< 0.19	$\cdots$
HH 52-53	9	0	< 0.26	$\cdots$
HH 54	12	0	< 0.22	$\cdots$
HH 75	9	0	< 0.17	$\cdots$
HH 77[b]	9	4	0.34±0.04	1.2±0.1
HH 240	11	10	0.45±0.06	0.6±0.1
HH 272	9	5	0.33±0.06	0.8±0.1

[a] Obs: n^o of positions observed, Det: n^o of positions with $\geq 3\sigma$ detections.

[b] HH 77 has an additional weak, 2σ detections, in other two positions.

$I(HCO^+) < 3\sigma_{mb}$ where σ_{mb} is the main beam RMS noise of the spectrum.

Eleven out of the twenty one objects surveyed (excluding HH 462 which seems to show emission from the dense circumstellar envelope around the exciting YSO), 52%, had HCO^+ (3–2) emission observed in at least one offset from the Herbig-Haro object. The HH objects observed were situated between 0.07 and 2.7 pc (projected distances) from their powering sources. The HCO^+ (3–2) emission associated with the dense circumstellar envelope around low mass protostars arises from a region of ~ 0.02 pc in diameter (Hogerheijde et al., 1997). Thus, we do not expect to be contaminated from the circumstellar molecular component. Of the sample no source further than 1 pc away from its powering source produced emission in the surrounding areas. The quiescent region we observed was typically between 0.01–0.07 pc from the HH object. The size of the emitting regions has been estimated from the number of offset positions that see emission (with a beam size of $20''$ for HCO^+ (3–2)), although it is extremely important to note that emission may extend beyond the regions mapped, as in a number of cases emission is seen up to the edge of the observed region. Five of the regions with several positions observed show detection in only few positions (HH 38, HH 43, HH 240 and HH 337). This suggests that the emission comes from compact clumps, probably with diameter between ~ 0.03 to 0.07 pc. In HH 77 and HH 427 there is some evidence that the emission may be also compact (about half of the positions observed had HCO^+ emission). HH 211 and HH 464 show emission in all the positions observed, implying an emission scale of ~ 0.1 pc or larger. For the SEST observations, if HCO^+ (3–2) was seen, then in all cases $H^{13}CO^+$ (1–0) was also seen. In HH 240 and HH 38 the $H^{13}CO^+$ (1–0) emission is more extended than the HCO^+ (3-2) line. Because of the lower critical density for the lower J rotational transition, this is an indication that the $H^{13}CO^+$ line is tracing lower density gas.
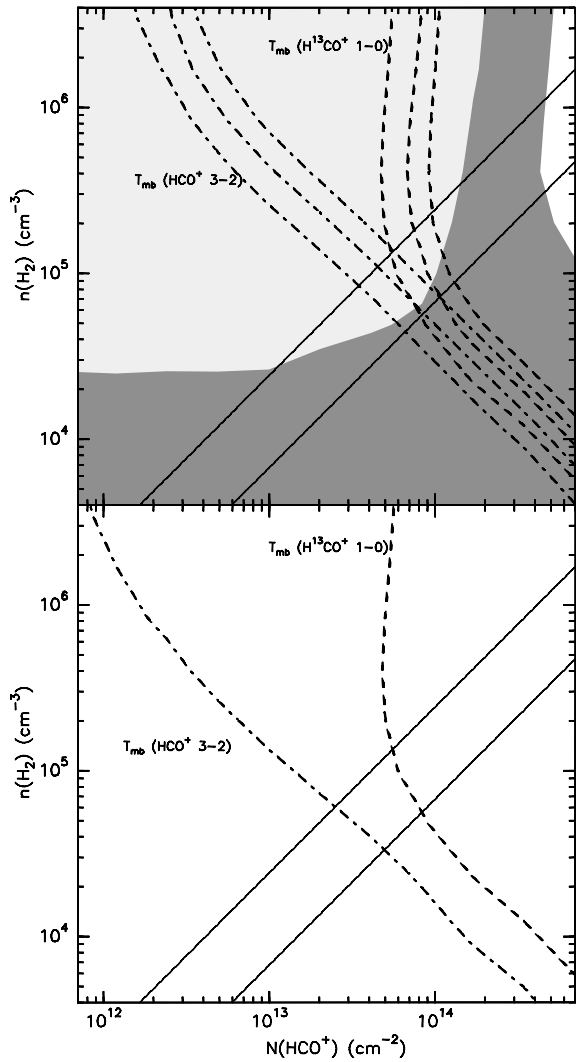
Fig. 14. *Top panel:* Plot of the set of RADEX solutions in the $N(HCO^+)$–$n(H_2)$ plane for HH 38 assuming a kinetic temperature of 10 K and a Gaussian source with a FWHM of 30″ or 0.07 pc. The dotted-dashed lines show the range of solutions for the observed intensity of the HCO^+ 3–2 line (including the uncertainties and taking into account the filling factor for the assumed size). The dashed lines shows the solutions for the $H^{13}CO^+$ 1–0 line. The grey area is the range of solutions for the observed line ratio for these two lines. The solid line shows the range of solutions for equation 1, for an HCO^+ abundance in the 2 to 5×10^{-9} range. *Bottom panel:* Similar to the top panel but for an observed intensity of 0.5 and 0.2 K for the HCO^+ 3–2 and $H^{13}CO^+$ 1–0 line, respectively. Higher values of the line intensities should appear above these lines.

4. Discussion and conclusions

4.1. The origin of the emission

The targets with detected HCO^+ (3–2) emission have sizes of about $\lesssim 0.1$ pc, except for those where the coverage was not enough to constrain the size (see previous section). However, this alone is not enough to state that the emission is coming from dense and small clumps or condensations within the dark

molecular cloud. In order to investigate if this is the case, we derived the density of the molecular gas traced by the HCO^+ for HH 38, a region where we have the two isotopologues and that shows compact emission. The gas volume density can be estimated in the following way:

$$n(H_2) \simeq \frac{N(HCO^+)}{X(HCO^+)} \frac{1}{L}, \qquad (1)$$

where L is the scale length of the emission, and $N(HCO^+)$ and $X(HCO^+)$ are the average values for the clump of the HCO^+ column density and the HCO^+ abundance relative to H_2, respectively. We adopt a length scale of $L = 0.07$ pc, which is roughly the diameter found for the HCO^+ (3–2) emission in HH 38. We adopt an HCO^+ abundance from 2 to 5×10^{-9}, values similar to those found in other HH objects (Girart et al., 2005; Viti, Girart, & Hatchell, 2006). We used the RADEX code (van der Tak et al., 2007), a non-LTE molecular radiative transfer in an isothermal homogeneous medium, to derive the HCO^+ (3–2) and $H^{13}CO^+$ (1–0) line intensities for a kinetic temperature of 10 K and for the adopted length scale (to include the filling factor correction in the derived RADEX intensities). As shown in Figure 14, the observed line intensities of HH 38 can be accounted for densities roughly near 10^5 cm^{-3}. In addition, if we consider that the detection threshold of our observations are $\simeq 0.5$ K and 0.2 for the HCO^+ (3–2) and $H^{13}CO^+$ (1–0), respectively, then for the same aforementioned conditions, the density of the detected emission should be higher than $n(H_2) \gtrsim 3 \times 10^4$ cm^{-3} (see Fig.14).

In any case, the lower limit derived for the volume density is clearly higher than the average density in molecular dark clouds, expected to be $\sim 10^3$ cm^{-3} (e.g. Loehr et al. (2007)). In addition, it should be noted that for most of the detections, the emission is quite far from the powering source of the HH object, so the contribution of the dense core around the YSO to the derived volume density is negligible. We conclude therefore that the bulk of the observed emission is indeed arising from small, compact, dense clumps with a minimum density of 3×10^4 cm^{-3}.

4.2. Estimation of clumpiness

It may be possible, at least in principle, to make an estimate of the clumpiness of molecular clouds from observations of HCO^+ emission in the vicinity of Herbig-Haro objects. Here, we indicate one method by which this estimate might be made. Of course, there are several caveats that must be accepted in attempting to do this. Firstly, the observed HCO^+ emission may be misleading in the sense that molecular clouds may contain filamentary or sheet-like structures that only appear to be clumpy because of their morphology; in such a case, the clumps may have no real significance. Secondly, the high-density emitting gas described in this paper may not be representative of the entire cloud, but only of a small region close to the HH object.

At present, there is rather limited evidence from high spatial resolution studies of the structure of molecular clouds. Morata, Girart, & Estalella (2003, 2005) made interferometric molecular line observations of a restricted region (about 0.7 pc × 0.7 pc) of the molecular cloud L673. When combined with

single-dish observations of the same region, the observations indicated that this limited region is populated by 15 resolved and distinct clumps of diameters less than about 0.1 pc and with gas number densities larger than 1×10^4 cm^{-3}. The clumps are transient and show evidence of time-dependent chemistry. Peng et al. (1998) and Takakuwa et al. (2003) found similar results for a region of the molecular cloud TMC-1.

These observations are limited to small regions of molecular clouds. As discussed in Section 1, there is, however, indirect evidence that supports the idea that clumps may be widespread in molecular clouds (Garrod et al., 2006).

Even if subsequent observations show that clumps are confined to restricted regions of molecular clouds, the distribution of matter in those regions is of interest, since the denser parts of the gas have the potential for low-mass star formation. We now proceed to make estimates of clumpiness on the assumption that discrete transient clumps are present in the vicinity of an HH object that is accompanied by HCO$^+$ emission. Whether or not the inferred measures of clumpiness should be applied to the entire cloud, in each case, will depend on the outcome of future interferometric observations of molecular clouds.

From our survey, one can derive a very rough statistical measure of clumpiness by considering the number of HCO$^+$ detections: the first consideration to make is that of the 21 objects observed (excluding HH 462) we had a positive detection in at least one position for $\sim$ 50% of the objects implying that, roughly, one in two HH objects is moving through a clumpy medium. Note that our survey probably did not cover all the regions that may emit strong HCO$^+$ for each object, hence this estimate may in fact be a lower limit.

Taylor & Williams (1996) suggested that an estimate of the mean linear separation between clumps detected near HH objects is given by

$$\left[\frac{l}{\text{cm}}\right] = 10^{17}\left[\frac{v}{30\,\text{km s}^{-1}}\right]\left[\frac{t}{100\,\text{yrs}}\right]\left[\frac{f}{0.1}\right]^{-1} \qquad (2)$$

where v is the velocity of the HH object, t is the duration of the anomalous emission from the irradiated clump, and f is the fraction of jets that have these clumps associated with them. For present purposes we adopt equation (2). The value of t is unconstrained in equation (2). We make a crude estimate of t by arguing that it is the time for the HH object to travel a distance equivalent to the clump diameter. For the clump size of $\sim$ 0.07 pc as measured for HH 38 (see Section 4.1) and for the canonical velocity in equation (2) this gives a value of t of roughly 2×10^3 yrs, that is consistent with a detailed dynamical study of the time evolution of clump chemistry (Christie et al. submitted). With $t = 2r/v$, then equation (2) gives $l = 2r/f$. For the clump diameter of HH 38, l is then 0.14pc. An estimate of the area filling factor, f_A, is $(r/l)^2$, i.e. $(f/2)^2$. with $f = 0.5$, then $f_A = 6\%$ for this example. Of course, this estimate is uncertain, but it is clear that an estimate can be made along these lines. An estimate of f_A from the observational data of Morata et al. (2005) suggests that f_A in L673 should be about 30%.

4.3. Conclusions

We have performed a large scale survey of HCO$^+$ (3–2) ahead of a sample of 22 sources, where no previous HCO$^+$ emission had been seen. Ten sources showed emission in HCO$^+$ (3–2) and when H^{13}CO$^+$ (1–0) observations were possible emission was also always seen. These clumps have velocities in line with the V$_{LSR}$ of the cloud, narrow linewidths of $\lesssim$ 1 km s^{-1} and hence they seem dynamically unaffected by the jet. The gas number densities of these clumps are close to 2 orders of magnitude higher than the mean density of molecular clouds ($n(\text{H}_2) \sim 10^5$ cm^{-3} for the case of the HH 38 region); this implies that these clouds may be highly heterogeneous at scales of less than 0.1 pc.

Our attempt at studying clumpiness by the use of HCO$^+$ demonstrates that it is possible, in principle, to use Herbig-Haro objects as probes of clumpiness in molecular clouds. Ultimately, future combined mm (mainly 3 mm) interferometric and single dish observations at relatively large scales with high sensitivity are required to fully determine the mass spectrum of the clumps, in a similar way of the work done by Morata et al. (2005). While we do not here attempt any explanation for the origin of molecular clumpiness, if slow-mode MHD waves (Falle & Hartquist, 2002) and MHD turbulence (Ballesteros-Paredes et al., 2007) are responsible for this highly heterogeneous medium, this mechanism should be such that within the clumps the non thermal linewidth is of the order or less than 1 km s^{-1}.

Our conclusions regarding measures of clumpiness should be qualified by the following remarks. The detection of enhanced HCO$^+$ emission close to the HH object enables us to estimate clumpiness only in the regions where high density gas is present, and may not represent the clumpiness throughout the cloud. Other observational approaches (e.g. Morata et al. 2003, 2005; Peng et al. 1998) detect clumpiness, but their studies are also of relatively small regions of molecular clouds. We cannot, therefore, conclude that the clumpiness estimate we have made is applicable to the entire molecular cloud. However, we note a modelling approach (Garrod et al. 2006) suggests that the clumpiness should be found throughout the molecular cloud.

Finally, it is implicit throughout this work that the clumpy structure is of essentially discrete parcels of relatively dense gas. This may not be the case; it is possible that the denser gas is in filaments rather than discrete clumps. The highest resolution maps of molecular clouds available (Morata et al. 2005 for L673) do seem to suggest separate structures, but of course unresolved material may also be present. Our assumption of discrete clumps is, therefore, plausible, but our estimates would have to revised if further evidence supports the filamentary nature of cloud structure.

References

Alten V. P., Bally J., Devine D., Miller G. J., 1997, IAUS, 182, 51P

Aspin C., Reipurth B., 2000, MNRAS, 311, 522

Ballesteros-Paredes, J., Klessen, R. S., Mac Low, M.-M., & Vazquez-Semadeni, E. 2007, Protostars and Planets V, 63

Bally J., Devine D., Alten V., 1996, ApJ, 473, 921

Bally J., Devine D., Reipurth B., 1996, ApJ, 473, L49

Bally J., Devine D., Alten V., Sutherland R. S., 1997, ApJ, 478, 603

Bally J., Walawender J., Luhman K. L., Fazio G., 2006, AJ, 132, 1923

Carballo R., Eiroa C., 1992, A&A, 262, 295

Cohen M., 1980, AJ, 85, 29

Cohen M., 1990, ApJ, 354, 701

Davis C. J., Ray T. P., Eisloeffel J., Corcoran D., 1997, A&A, 324, 263

Dent, W. R. F., Cunningham, C., Hayward, R., et al. 1993, MNRAS, 262, L13

Eislöffel J., Mundt R., 1998, AJ, 115, 1554

Eislöffel J., 2000, A&A, 354, 236

Falle, S. A. E. G., & Hartquist, T. W. 2002, MNRAS, 329, 195

Garrod, R. T., Williams, D. A., & Rawlings, J. M. C. 2006, ApJ, 638, 827

Girart, J. M., Estalella, R., Ho, P. T. P., & Rudolph, A. L. 2000, ApJ, 539, 763

Girart J. M., Viti S., Estalella R., Williams D. A., 2005, A&A, 439, 601

Girart J. M., Viti S., Williams D. A., Estalella R., Ho P. T. P., 2002, A&A, 388, 1004

Haro G. 1953, ApJ, 117, 73

Herbig G. H., 1974, LicOB, 658, 1

Herbst W., 1975, AJ, 80, 212

Hodapp K.-W., Ladd E. F., 1995, ApJ, 453, 715

Hogerheijde, M. R., van Dishoeck, E. F., Blake, G. A., & van Langevelde, H. J. 1997, ApJ, 489, 293

Knee, L. B. G. 1992, A&A, 259, 283

Langer, W. D., & Penzias, A. A. 1993, ApJ, 408, 539

Lefloch, B., Cernicharo, J., Cabrit, S., & Cesarsky, D. 2005, A&A, 433, 217

Löhr, A., Bourke, T. L., Lane, A. P., Myers, P. C., Parshley, S. C., Stark, A. A., & Tothill, N. F. H. 2007, ApJS, 171, 478

McCaughrean M. J., Rayner J. T., Zinnecker H., 1994, ApJ, 436, L189

Morata O., Girart J. M., Estalella R., 2003, A&A, 397, 181

Morata O., Girart J. M., Estalella R., 2005, A&A, 435, 113

Moriarty-Schieven G. H., Johnstone D., Bally J., Jenness T., 2006, ApJ, 645, 357

Noriega-Crespo A., 2002, RMxAC, 13, 71

Peng, R., Langer, W. D., Velusamy, T., Kuiper, T. B. H., & Levin, S. 1998, ApJ, 497, 842

Raga, A. C., & Williams, D. A. 2000, A&A, 358, 701

Reipurth B., Graham J. A., 1988, A&A, 202, 219

Reipurth B., Nyman L.-A., Chini R., 1996, A&A, 314, 258

Rudolph, A., & Welch, W. J. 1988, ApJ, 326, L31

Rudolph, A., & Welch, W. J. 1992, ApJ, 395, 488

Sahu, M., Sahu, K. C., & Pottasch, S. R. 1989, A&A, 218, 221

Schwartz R. D., 1977, ApJ, 212, L25

Schwartz R. D., 1977, ApJS, 35, 161

Schwartz R. D., 1978, ApJ, 223, 884

Stanke, T., McCaughrean, M. J., & Zinnecker, H. 2000, A&A, 355, 639

Takakuwa S., Kamazaki T., Saito M., Hirano N., ApJ, 584, 818

Taylor, S. D. & Williams D. A., 1996, MNRAS, 282, 1343

Torrelles, J. M., Rodriguez, L. F., Canto, J., et al. 1992, ApJ, 396, L95

van der Tak, F. F. S., Black, J. H., Schöier, F. L., Jansen, D. J., & van Dishoeck, E. F. 2007, A&A, 468, 627

Viti S., Girart J. M., Garrod R., Williams D. A., Estalella R., 2003, A&A, 399, 187

Viti S., Girart J. M., Hatchell J., 2006, A&A, 449, 1089

Wu J.-W., Wu Y.-F., Wang J.-Z., Cai K., 2002, ChJAA, 2, 33

Yan J., Wang H., Wang M., et al. 1998, AJ, 116, 2438